HHS Public Access

Author manuscript

Nat Neurosci. Author manuscript; available in PMC 2011 June 01.

Published in final edited form as:

Nat Neurosci. 2010 December ; 13(12): 1534–1541. doi:10.1038/nn.2670.

Thalamic Synchrony and the Adaptive Gating of Information Flow to Cortex

Qi Wang[1,2], **Roxanna M. Webber**[3], and **Garrett B. Stanley**[1]

[1] Coulter Department of Biomedical Engineering, Georgia Institute of Technology & Emory University, 313 Ferst Drive, Atlanta, GA 30332

[2] School of Engineering & Applied Sciences, Harvard University, 60 Oxford St., Cambridge, MA 02138

[3] Department of Neurobiology, Harvard Medical School, 220 Longwood Ave., Boston, MA 02115

Abstract

Although it has long been posited that sensory adaptation serves to enhance information flow in sensory pathways, the neural basis remains elusive. Simultaneous single–unit recordings in the thalamus and cortex in anesthetized rats reveal that adaptation differentially influences thalamus and cortex in a manner that fundamentally changes the nature of information conveyed about vibrissae motion. Utilizing an ideal observer of cortical activity, performance in detecting vibrissa deflections degrades with adaptation, while performance in discriminating between vibrissa deflections of different velocities is enhanced, a trend not observed in thalamus. Analysis of simultaneously recorded thalamic neurons does reveal, however, an analogous adaptive change in thalamic synchrony that mirrors the cortical response. An integrate–and–fire model using experimentally measured thalamic input reproduces the observed transformations. The results here suggest a shift in coding strategy with adaptation that directly controls information relayed to cortex, which could have implications for encoding velocity signatures of textures.

Keywords

adaptation; thalamocortical; vibrissa; tactile; ideal observer

Introduction

Adaptation is a ubiquitous property across a large variety of areas within different sensory pathways of the brain[1-6]. Although typically associated with an attenuation of neural activity resulting from a number of different biophysical mechanisms, adaptation is thought to

Correspondence should be addressed to: Professor Garrett B. Stanley, Coulter Department of Biomedical Engineering, Georgia Institute of Technology & Emory University, 313 Ferst Drive, Atlanta, GA 30332, Phone: 404.385.5037, garrett.stanley@bme.gatech.edu.

Author Contributions: Q.W. and G.B.S. conceived the experiments. Q.W., R.M.W. and G.B.S. designed the experiments. Q.W. performed the experiments. Q.W. and G.B.S. analyzed the data, and Q.W., R.M.W. and G.B.S. wrote the paper.

enhance the flow of information transmission in sensory pathways in complex environments[7]. Computational studies have quantitatively demonstrated that adaptation maintains information rates in the face of changes in the statistics of the sensory input[5, 6]. Consistent with these notions, psychophysical studies have shown that adaptation to a periodic tactile input enhances human performance in both amplitude and frequency discrimination[8-11]. The precise link between the changes in coding properties and the feature representation in the various stages of processing that underlies perception, however, remains poorly understood.

Due to the well–studied feed–forward anatomy, the thalamus is classically described as a relay station between the sensory periphery and the cortex. However, the complex dynamic interaction between the thalamic and cortical structures is perhaps the key element in establishing representations that ultimately result in perception of our sensory environment. It has been asserted that thalamic gating can shift coding properties of the pathway between *detecting* salient features of the sensory environment and *transmitting* details of the sensory environment[12, 13]. By taking the perspective of an ideal observer of thalamic activity and decoding elements of the sensory input, we have previously shown that high frequency thalamic bursting is selective for detecting salient features in the natural sensory input[14]. Short inter–spike intervals of single thalamocortical neurons[15] and synchronous activity across multiple thalamic neurons projecting to a common cortical target[16, 17] are significantly more likely to evoke spiking in the downstream cortical neuron, consistent with the notion of a “window of opportunity” for integration for the cortical cell[18]. It has recently been shown that adaptation strongly shapes thalamic synchrony[19] and dictates the window of integration of the recipient cortical target[20]. How this shapes not only how much, but what kind of information is conveyed to the cortex, is unknown.

Here, through simultaneous single–unit recordings in the ventral posteromedial (VPm) nucleus of the thalamus and cortical layer 4 in the rat vibrissa pathway during controlled vibrissa movements in the anesthetized rat, we show that sensory adaptation differentially influences thalamic and cortical activity in a manner that fundamentally changes the nature of the information conveyed about the sensory input. Specifically, from the perspective of an ideal observer of spiking activity, the cortical neurons exhibit a degraded performance in detecting vibrissa deflections with adaptation, while exhibiting an enhancement in discriminating between deflections of different velocities. Paired recordings in topographically aligned neurons in the VPm thalamus reveal no such trend in the projecting input to cortex, also reflected in putative monosynaptic pairings. Analysis of simultaneously recorded thalamic neurons does unveil, however, an analogous adaptive change in thalamic synchrony that mirrors the observations of cortical response magnitude. A simple leaky integrate–and–fire network model using experimentally measured thalamic input reproduces the observed transformations from thalamus to cortex. Taken together, the results here suggest an adaptive shift in the coding strategy with adaptation that has direct functional consequences regarding the nature of information relayed to cortex.

Results

Single–unit, extracellular recordings were made of putative excitatory neurons (Regular Spiking Units (RSUs) – Fig. 1a, left, for a typical RSU waveform) in layer 4 of the vibrissa region of the primary somatosensory cortex, in response to controlled deflection of the corresponding primary vibrissa (Fig. 1a, Supplementary Fig. 1 online for all cortical units in the main dataset of the study). Cortical neurons adapted strongly to persistent, ongoing sensory stimuli, as shown by the peri–stimulus time histogram (PSTH) of evoked activity from a typical neuron in Fig. 1b in response to a 12 Hz periodic vibrissa deflection pattern.

In response to these transient vibrissa motions, cortical neurons exhibited an exponential reduction in spike count from the stimulus onset (Non–adapted) to steady–state (Adapted), shown for a sample of cortical neurons in the top panel of Fig. 1c (n=30). The reduction in spike count from the Non–adapted to Adapted states was quantified by the Adaptation Ratio (ratio of Adapted spike count to Non–adapted, see Methods), which was 67% here, consistent with other studies using similar experimental methodologies[3], [4]. The reduction in spike count with adaptation was accompanied by a corresponding reduction in trial–to–trial spike count variance, as shown in the bottom panel of Fig. 1c. The relationship between the mean and variance was non–linear, following a sub–linear exponential rise to an apparent saturation (Fig. 1d, dashed curve; Supplementary Fig. 5 online).

Detection and the Ideal Observer

Taking the perspective of an ideal observer of the cortical response, we can ask to what extent we can detect the presence of a vibrissa deflection, and how this is affected by adaptation. The observer was asked to indicate whether or not a vibrissa deflection was presented following a cue marking the stimulus onset (Fig. 2a). This can be envisioned as discrimination between “signal” and “noise”, in the classical signal detection theory framework.

The observer was challenged with this question before (Non–adapted) and after (Adapted) the pathway was presented with an adapting periodic vibrissa deflection. The ideal observer made the decision based on the summed activity across multiple trials, assumed to represent the aggregate population spike count[21], [22] (see Methods). An example of the corresponding distributions in the presence (signal) and absence (noise) of a vibrissa deflection for a typical cortical RSU is shown (Fig. 2b). Plotted are the parametric fits of the experimentally measured distributions (Supplementary Fig. 3a online). The signal in this case was a weak punctate vibrissa deflection of 50 deg./sec. The spike count distributions for the Non–adapted case are shown (top panel). The mean population spike count was of course larger for the signal (black) than for the noise (gray), but both exhibited some degree of variability, leading to overlap in the distributions. Classical signal detection involves the selection of a threshold, above which the response is classified as signal, and below which as noise. The area under the response distribution to the right of the threshold when a signal was actually present (black) is the probability of a correct detection (“hit”), whereas the corresponding area under the response distribution in the absence of signal (gray) is the probability of an incorrect attribution of the observed response to signal when it was actually noise (“false alarm”). Given the effect of adaptation on the spike count, we expected that the mean

population spike count for the vibrissa deflection would decrease, as shown in the bottom panel of Fig. 2b. In addition to the mean population spike count, adaptation decreased the variance and significantly altered the noise distribution (spontaneous activity). Together, these changes affected the degree of overlap between the signal and noise distributions.

The performance of the observer was quantified using a receiver operating characteristic (ROC) analysis[21], [22], which captures the probability of false alarms versus correct detections as a function of the choice of thresholds (Fig. 2c). Because the performance varies with the choice of threshold, the total area under the ROC curve (AUROC) was used as a single metric of overall performance, where a value of 1 indicates a false alarm rate of 0 and a hit rate of 1, and a value of 0.5 indicates chance. For this particular cortical neuron, for a given angular velocity, the AUROC was significantly larger for the Non–adapted (dotted) state as compared to the Adapted (solid). Shown is a scatter plot of performance in the Non–adapted state versus the Adapted state for the larger sample (n=30) for the lowest velocity presented (Fig. 2d), exhibiting a significant degradation in detection performance with adaptation (left side of Fig. 2e, $p<10^{-19}$, Wilcoxon signed–rank test). A control analysis showed that this effect was not due to the sub-linear decrease in variance with adaptation (Fig. 2e, right; see figure caption and Supplementary Note 1 online). Note that for Fig. 2e, the detection performance was evaluated for a range of probe velocities, exhibiting an overall higher level of performance as compared to the scatter plot for the low velocity probe in Fig. 2d.

Discrimination and the Ideal Observer

Again taking the perspective of an ideal observer of the cortical response, we can ask to what extent we can discriminate between different sensory inputs, and how this is affected by adaptation. The observer was asked to discriminate between vibrissa deflections of different velocities (Fig. 3a).

The observer was challenged with this question in the presence (Adapted) or absence (Non–adapted) of previously adapting periodic vibrissa deflections. Shown are the velocity sensitivity curves across the sample of cortical neurons, in the Non–adapted (dotted) and Adapted (solid) states (Fig. 3b). It is clear that the adaptation attenuated the response magnitude for all stimuli (velocities). However, the difficulty of the task of the observer depended upon the overlap in distributions of the responses to each of the velocities. Shown is an example of the response distributions of a particular cortical neuron in response to five different stimuli (s1, s2, s3, s4, s5; Fig. 3c), which are five different angular velocities of vibrissa deflection (50, 100, 300, 600, 1200 deg./sec, respectively). Note that the stimulus design held the duration of the punctate stimulus fixed, and thus the peak amplitude of the deflection covaried with the velocity (see Methods). Plotted are the parametric fits of the experimentally observed distributions (Supplementary Fig. 3b online). We can immediately see that for this example cell in the Non–adapted case (top), the spike counts were relatively high, but the distributions were highly overlapped, and even unordered. In contrast, in the Adapted case (bottom), the spike counts were attenuated, but the distributions became more separated and ordered.

To quantify the effects of this transformation on the performance of the ideal observer in discriminating between different deflection velocities, we used a Bayesian decoder to estimate the most likely velocity presented from the observed cortical response, given a uniform prior (i.e. each velocity was presented with equal probability). The inset in Fig. 3c shows the performance matrix, which displays the probability of inferring a particular velocity (columns) for each of the actual velocities presented (rows). The overall metric of performance reflects the fraction of correctly identified stimuli (chance would be 20% or 0.2). In contrast to the detection task, the observer was significantly better at discriminating between different velocities in the Adapted state, as compared to the Non–adapted state (Fig. 3d). This result is further summarized in Fig. 3e, where the discrimination performance was significantly better in the Adapted state as compared to Non–adapted ($p<3\times10^{-4}$, n=30, Wilcoxon signed–rank test). The control analysis reveals that the change in performance with adaptation observed in the data was not a trivial consequence of the attenuated response in the Adapted state, but instead relied on the non–uniform changes in the separation between the distributions with adaptation (see figure caption and Supplementary Note 1 online).

In addition to the obvious adaptation effects on the spike count, the average overall shape of the sensitivity curve changed with adaptation, from a step–function form to that which exhibited a more gradual change in response with increased stimulus strength (Fig. 3b). The adaptation thus provided sensitivity over the range of angular velocities tested here. Taken together, the results of the Detection and Discrimination performance analysis show that adapting cortical neurons switched from a state in which detection was favored to a state in which discrimination was favored. Importantly, in an additional set of experiments, we found that adaptation enhanced discriminability between deflections of the vibrissa in different angular directions, pointing to a general phenomenon (Supplementary Note 3 and Supplementary Fig. 6 online).

Thalamic Input

Given the observations regarding the switch in performance with adaptation in the cortical response, it is important to ask how these properties arise. It may simply be the case that the cortex was trivially inheriting these properties from the projecting thalamic input. Neurons in the ventral posteromedial nucleus (VPm) of the thalamus do also adapt in response to persistent, ongoing sensory input in a manner similar to that in cortex, albeit to a lesser degree. Each of the cortical neurons in Figs. 1–3 was recorded while simultaneously recording from a topographically aligned VPm neuron (i.e. in the homologous barreloid, see Fig. 1a inset for typical VPm spike waveform, and Supplementary Fig. 2 online for all thalamic units in the main dataset of the study). Shown is a PSTH for a typical VPm neuron and the mean decay in VPm spike count in response to the same 12 Hz repetitive stimulus (Fig. 4a; n=32; for 2 recording sessions, two VPm units were recorded on separate electrodes of the multi–electrode positioned in thalamus). Note that the VPm PSTH exhibited a fairly rapid decrease in amplitude, whereas the spike count decay was much more gradual, consistent with previous observations[23].

Although the adaptation response was qualitatively similar to the cortical neurons, VPm neurons exhibited weaker adaptation and a correspondingly larger adaptation ratio of 80% (as compared to 67% for the cortical RSUs (n=30) in Fig. 1c, $p<0.01$, Mann–Whitney U test) – see inset. An ideal observer of the VPm spike count was then challenged with the same detection and discrimination tasks as above. Although the VPm detection performance did degrade with adaptation due to the decreased spike count ($p<0.01$, n=32, Wilcoxon signed–rank test; Supplementary Fig. 7 online), the adaptation produced no change in discrimination performance in contrast to observations in cortex (Fig. 4b; $p=0.19$, n=32, Wilcoxon signed–rank test). In contrast to their cortical counterparts, the velocity sensitivity curves for the VPm neurons exhibited only an overall scaling of the magnitude of the spike count with adaptation (Fig. 4c, dotted versus solid), as opposed to a fundamental change in shape of the sensitivity in cortex that gave rise to the change in performance (Supplementary Fig. 9 online).

To rule out the possibility that the observed discrepancy between changes in thalamic and cortical discrimination performance with adaptation was due to experimental methods or selection bias in the neural recordings, we analyzed the simultaneously recorded VPm and cortical activity in a pair–wise manner. First, a small subset of the thalamocortical pairs was conservatively identified as having monosynaptic connectivity (i.e. the recorded VPm neuron served as direct input to the layer 4 cortical neuron, crosses in Figs. 3d and 4b). This assessment was performed using spike cross–correlation analysis in the presence of a very weak vibrissa stimulation, as described in the Methods [24, 25].

Shown is an example of the shuffle–corrected spike cross–correlogram for a typical pair, with the raw cross–correlogram shown reflected about the horizontal axis (Fig. 5a). The dotted line represents a >99% confidence interval (3 standard deviations) on an uncorrelated process. The emergent peak at approximately 2 ms was consistent with monosynaptic connectivity across the thalamocortical structures[15, 24]. The inset shows the average correlograms across the subset of pairs we identified as monosynaptically connected (n=8 pairs). For this subset of pairs, the discrimination performance was significantly better in the Adapted state as compared to the Non–adapted state for the cortical cell (Fig. 5b, left) ($p<0.007$, Wilcoxon signed–rank test), while the VPm cell exhibited no difference (Fig. 5b, right) ($p=0.84$, Wilcoxon signed–rank test). The primary result here thus held for the conservatively identified connected pairs. Further, it is likely that many of the other recorded pairs were also connected pairs, but did not meet the stringent requirements imposed here[25]. Shown is the pair-wise percent change in discrimination performance from the Non–adapted to Adapted state for each of the simultaneously recorded VPm and cortical pairs (Fig. 5c), with the identified monosynaptically connected pairs shown in gray, showing little or no trend in performance for the VPm while showing an enhanced performance for the cortex. The increase in cortical discrimination performance with adaptation was significantly greater than that in VPm (comparison of performance ratios, $p<0.001$, Student's t–test, see Methods).

Thalamic synchrony affects cortical performance

The above results suggest that the cortical shift in performance was not trivially inherited from the projecting thalamic input. However, this does not completely preclude an explanation of the cortical response properties from the thalamic population input. Timing across the thalamic population has been shown to be a critical component in establishing feature selectivity in cortex[26]. In a separate set of experiments, a multi–electrode was utilized to record simultaneously from VPm pairs within the same barreloid in response to the adapting stimulus (see Methods). As the VPm adapts in response magnitude (spike count), we observed a desynchronization of the thalamic response. The mean synchrony decreased with the adapting stimulus (Fig. 6a; n=19 VPm pairs), where synchrony was defined as the central area under the spike cross–correlogram (+/− 7.5 ms, see Methods and Supplementary Note 4). The synchrony defined here is the probability, given a spike of one VPm neuron, of observing a spike from the other VPm neuron in the pair within +/− 7.5 ms (solid is from raw correlogram, dotted is from trial shuffled correlogram; Supplementary Fig. 8 online).

The synchrony across VPm neurons was also modulated by the vibrissa deflection velocity. The thalamic synchronies for the different velocities are denoted by the tick marks on the left (Non–adapted) and right (Adapted) of Fig. 6a, labeled as stimuli s1–s5. The different velocities elicited greater variation in the synchrony across the pairs in the Adapted as compared to Non–adapted states. This effect is shown in more detail in Fig. 6b, where the velocity effects on synchrony are presented for both the Non–adapted and Adapted states (n=19 VPm pairs). The adaptation acted to attenuate thalamic synchrony, while simultaneously increasing the sensitivity of thalamic synchrony to velocity. This can be seen in the shape of the synchrony curve in the Adapted state, reminiscent of the cortical spike count curve shown in Fig. 3b. Although the presence and importance of noise correlations has recently been described for this pathway[19], the effects here were largely stimulus–driven, as the noise correlations were comparatively small and relatively insensitive to deflection velocity (linear regression, p=0.32 for Non–adapted and p=0.35 for Adapted, see Supplementary Fig. 8 online).

The importance of the above observation becomes clear in considering the role of timing across thalamic neurons in determining the response of the downstream layer 4 cortical target. Consider the cartoon illustration in Fig. 7a. Shown is the relative timing of firing across a small population of VPm neurons, and the effects of the stimulus strength on the degree of synchronization of these responses.

Previous studies of the thalamocortical circuit have demonstrated that adaptation modulates the integration window of the thalamic influence on the recipient layer 4 neurons[20]. Specifically, adaptation delays the arrival of feedforward inhibitory inputs, increasing the window of opportunity for feedforward excitatory thalamic input. The integration window of the recipient cortical cell is illustrated with the shaded region for both the Non–adapted and Adapted states (12 +/− 2 ms Non–adapted, 22 +/− 2 ms Adapted[20]). In the Non–adapted case, the changes in the synchronization with stimulus strength are small relative to the integration window, thus leading to a relative insensitivity of the cortical response to stimulus strength (velocity). In contrast, in the Adapted case, although the integration

window is wider as compared to the Non–adapted state, the overall synchrony is less, and more importantly, the changes in synchrony with changes in deflection velocity are pronounced. This leads to spiking of some of the VPm cells outside the window of integration, and thus a less efficacious input to drive the recipient cortical target.

Detection, Discrimination, and Window of Opportunity

The above qualitative assertion can be demonstrated quantitatively through the use of a simple leaky integrate–and–fire model of the cortical response to incoming VPm inputs (Fig. 7b). The degree of synchrony was nearly identical across simultaneously recorded VPm pairs when the trials were randomly shuffled relative to each other (Fig. 6a), suggesting that the VPm pairs had very weak noise correlations compared to the stimulus driven correlations (dotted curve in Fig. 6a). Although the weak pair–wise correlations might play a role in the behavior of the network at a larger scale[27], here we focused on the stimulus driven correlations (see Discussion). In the model, a random selection of trials across all recorded VPm neurons was used as a surrogate for the population VPm response on a single trial. The thalamic population input corresponding to a particular deflection velocity (s1–s5) was generated from 10 trials of experimentally recorded VPm activity corresponding to that particular velocity, randomly drawn across all recorded VPm cells and trials. The VPm population firing produces excitatory post–synaptic currents (EPSCs) that were spatially summed, capturing the total synaptic drive of the cortical RSU. This input was integrated, yielding an instantaneous measure of the membrane potential of the model cortical cell. Action potentials were generated when the potential crossed a threshold, at which point the integrator was reset (see Methods for a description of the model membrane properties). The "window of opportunity" was assumed to follow that described previously, where adaptation delays the arrival of feedforward inhibitory inputs, increasing the window of opportunity for feedforward excitatory thalamic input to generate downstream suprathreshold activity[20]. In the Non–adapted state, the recorded VPm activity is sufficiently synchronous as not to affect the cortical response. The resulting cortical response in the Non–adapted state thus reflected primarily the fraction of VPm units firing. Since the VPm spike count was relatively insensitive to vibrissa deflection velocity in the Non–adapted state, the cortical spike count was also relatively insensitive to velocity. In contrast, however, in the Adapted state, the VPm input was less synchronous, and the degree of synchrony was more sensitive to the velocity as compared to the Non–adapted state (Fig. 6b). Weaker stimuli resulted in loss of synchrony. As a result, despite the lack of VPm spike count sensitivity to velocity, the model cortical spike count was sensitive to velocity, as shown in Fig. 7c. Note that the model prediction was quite similar to the experimental findings in Fig. 3b (Supplementary Figs. 9b,d online). As a result, there was an increase in discrimination performance from the Non–adapted to Adapted states (Fig. 7d; $p<2\times10^{-4}$, n=30 simulated neurons, Wilcoxon signed–rank test), as we observed in experimental data (Fig. 3e).

To confirm that the enhancement of cortical discrimination performance was due to adaptation of thalamic synchrony, and to rule out the contribution of VPm spike count in the observed phenomena, we performed a control analysis. Specifically, spikes were removed from the Non–adapted VPm responses according to the observed thalamic adaptation ratio of 80% (i.e. 20% of the spikes were removed) to create the hypothetical Adapted VPm input

for the Adapted state. In other words, we preserved the experimentally observed VPm spike count in the adapted state, but eliminated adaptation effects on the synchrony. The “control” Adapted VPm sensitivity curve thus was the same as the experimentally observed curve in Fig. 4d (solid), but the synchrony matched the Non–adapted case (dotted line in Fig. 6b). Using this to drive the model, we found that this dramatically degraded the discrimination performance of the resultant cortical model output (Control case in Fig. 7d, not significantly different from the Non–adapted case ($p=0.43$, Wilcoxon signed–rank test)). Thus, we conclude that the adaptation effect on thalamic synchrony was the key element in the shift in cortical coding strategy with adaptation.

Discussion

Our results provide a direct link between the long–observed phenomenon of enhanced sensory performance with adaptation and the underlying neurophysiological representation in the primary sensory cortex. Here, we show that adaptation not only serves to enhance discriminability of vibrissa deflection velocities, but also to enhance discriminability of deflection angle (Supplementary Note 3 and Supplementary Fig. 6 online), pointing to a general phenomenon. It has long been postulated that sensory adaptation serves to enhance information flow in sensory pathways[7]. Psychophysical studies have indeed shown that adaptation to a periodic tactile input on the skin surface enhances spatial localization in a two point discrimination task in humans[10], presumably through engaging lateral inhibitory mechanisms serving to better spatially localize the cortical activation. Further, adaptation to periodic tactile input has also been shown to enhance amplitude[9] and frequency discrimination[8] in humans. Although the perceptual effects of adaptation have been studied in some detail, the link to the underlying neurophysiology has historically been much less clear. In contrast to previous studies focusing on how adaptation influences *how much* information is being transmitted by the pathway[5], [6], here we show that it is also important to reframe the question: *What is information being transmitted about?*

Neurons in the sensory cortices adapt their mean firing rates to ongoing stimuli in a number of different pathways. However, in the face of dynamic sensory input there is a complex, evolving interplay between excitatory and inhibitory sub–populations of cortical neurons that affects the population activity across the thalamocortical structures in a more subtle, and computationally rich, manner[23], [28]. For example, the excitatory and inhibitory inputs to cortical cells dynamically adapt in response to a periodic stimulus[3], [20], [29]. This interplay between excitation and inhibition at the level of the cortex provides a “window of opportunity” for generating supra–threshold cortical responses[20] that matches the dynamic range of the stimulus. During repetitive stimulation, feed–forward inhibition onto cortical excitatory cells decreases, due to depression of both thalamocortical and cortico–cortical synapses, leading to an increase in the integration window of excitatory responses[20]. Given that the effects of adaptation are strongly dependent upon the nature of the adapting stimulus[19], [23], it remains to be seen how adapting inputs of varying strength and statistical structure[30] would shape the cortical sensitivity. Taken together, our results here suggest a dynamically evolving relationship between thalamic timing precision and its impact on cortex that could be a key element in the observed perceptual effects of adaptation.

Neuronal synchrony is thought to play a major role in sensory function and cognition[31], and such precise timing has been implicated in playing a key role in neural coding[28], [32]. Thalamic synchrony has been previously proposed as an important component in generating cortical response properties in the vibrissa pathway[18], [33]. In response to a single sensory stimulus, the temporal precision of thalamic input influences the cortical response to a greater extent than the overall thalamic firing rate[18], and high velocity vibrissa stimuli induce synchronous thalamic firing within a barreloid[19], [25]. Here, we show that although the cortical response is indeed sensitive to stimulus intensity in the Non–adapted state[18], stimulus intensity can modulate thalamic synchrony more effectively in the Adapted than Non–adapted state. This results in better discrimination performance based on downstream neural firing activity due to enhanced sensitivity in the Adapted state. Although the precise timing of thalamic firing is thought to be primarily generated by the strong inputs from trigeminal brainstem afferents, the adaptation of inhibitory input from thalamic reticular nucleus (nRT) also likely modulates VPm synchrony[34].

It has recently been shown that weak pair–wise correlations across neurons can have important implications for the large–scale network[27]. However, the effect of pair–wise correlations on coding strategies is still very much in debate[35], [36], and the implications in the context of adaptation are unclear. We should note that the measurements we provide here are comparative in nature. That is, we characterize the shift in pair–wise correlations from Non–adapted to Adapted states. We implicitly assume that the relationship between the weak pair–wise correlations and the coding strategies of the large–scale network would be preserved through adaptation, but this remains an open question.

Rats and other rodents rely extensively on their tactile sense to navigate and perceive the external world. It has been shown that this sensory modality is endowed with the capability for surprisingly fine texture discrimination[37], [38]. When in contact with a textured surface, the vibrissae resonate transiently during discrete, high–velocity “slip–stick” events[39]-[41]. The rate/pattern of these high–velocity vibrissa transients varies with the properties of the texture and self–motion, resulting in patterns of temporally precise, stimulus locked spiking activity, described as a “kinetic signature” of the textured surface[42]. Thus the discrimination between different textures potentially involves the discrimination between patterns of velocity transients, based on corresponding patterns of cortical activation. In the natural environment, rats use foveal whisking to identify/palpate objects of interest[43], generating high frequency vibrations of the vibrissae (hundreds to thousands of Hertz) for hundreds of milliseconds[38]. Such persistent activation of the pathway may put the brain in an Adapted state, resulting in an enhanced discriminability of the relevant features of the texture. In addition to surface texture properties, the vibrissa system also provides information to the animal that is useful for object localization[44], aperture discrimination[45], and stimulus detection[22] and discrimination[46], in many cases involving the inference of a single transient contact, such as that presented in the detection task in this study. Given this dichotomy, it has been proposed that the lemniscal and paralemniscal pathways separately process vibrissa motion in parallel for texture coding and object–contact, respectively[1]. The thalamic data shown here were identified as VPm in origin, and thus part of the lemniscal tract, based on stereotaxic coordinates and response latencies (Supplementary Note 5). While it is not presently known if the seemingly disparate types of sensory information involved in discrimination and

contact/detection are mutually exclusive behaviorally, nor is it known to what extent the pathways interact as the self–motion of the animal shapes the sensory input in a continuous manner[47], our study does demonstrate that the lemniscal pathway preserves sufficient information for dynamically switching between different coding strategies in behavioral contexts.

The properties of the sensory input play a large role in controlling overall activation and timing precision across neurons in the local populations[48], suggesting a potential role for thalamic synchrony in controlling information flow to cortex in the non–stationary natural sensory environment[32]. However, the thalamocortical network is also strongly influenced by non–peripheral inputs that are associated with states of arousal. Specifically, activation of the reticular formation influences thalamus and cortex both directly and indirectly. Recently, it was shown that electrical stimulation of the basal forebrain served to enhance discriminability across the thalamocortical circuit[49], presumably through modulations in thalamic synchrony. Neurotransmitters associated with arousal act to depolarize the thalamus, shifting the firing properties[50], and increasing the spontaneous firing rate of thalamocortical neurons[51]. Increased thalamic activity associated with arousal leads to an "adapted" state in cortex characterized by low background firing, higher signal–to–noise, and sharpened receptive fields[51]. Given the differences in thalamocortical activity between the anesthetized and awake animal[50],[51], it remains an open question as to how the neural phenomenon described here is impacted by wakefulness and higher level, top–down attentional processes. Nevertheless, adaptation to a periodic tactile input has been shown to enhance spatial localization and frequency discrimination in humans[8-11].

Although the issue of rate versus temporal coding has been vigorously debated in the literature, currently there is fairly widespread agreement that the various pathways in the brain likely operate on a range of timescales[52], and that the relevant timescales likely change with time and context. The timescale of firing activity across upstream neural populations is transferred to downstream neural activity by the dynamics of synaptic integration across the brain regions, and thus the range of timescales of synaptic integration ultimately determines the relevant timescales of the neural code. The results here suggest that with respect to stimulus strength (angular velocity), the thalamic population operates with a temporal code that is transformed to a rate code across the thalamocortical synapse. Moreover, the dynamics of thalamocortical integration change in a complex way with adaptation[20], which, along with modulation of synchronization across the thalamic population, leads to a dynamic gating of information flow to cortex, consistent with the hypothesis that adaptation in the rat vibrissa system could serve to switch from a mode that facilitates detection to one that facilitates discrimination. Studies pairing electrophysiological recordings with behavior that permit the direct comparison of neurometric and psychometric performance suggest a complex relationship between the timecourse of cortical activity and perception[53]. Although it is not likely that cortical layer 4, or even S1, is solely responsible for generating perceptions, the emergence of feature selectivity across the thalamocortical synapse forms the constituent elements upon which perception is ultimately built.

Materials & Methods

Surgery and preparation

Forty female adult Sprague Dawley rats (220–330 g) were used in the study. All procedures were approved by the Institutional Animal Care and Use Committees at Harvard University and Georgia Institute of Technology. Briefly, rats were sedated with 2% vaporized isoflurane and anesthetized with sodium pentobarbital (50 mg/kg, i.p., initial dose); Supplementary doses were given as needed to maintain a surgical level of anesthesia, confirmed by measurements of heart rate, respiration and eyelid/pedal reflexes to averse stimuli (toe or tail pinch). Body temperature was maintained at 37 °C by a servo–controlled heating blanket (FHC, Bowdoinham, ME). The animal was mounted on a stereotaxic device (Kopf Instruments, Tujunga, CA) on a floating table in preparation for the surgery and subsequent recordings. Atropine (0.5 mg/kg, s.c.) was injected, and 2% Lidocaine solution was applied to the tissue on top of the head. A small craniotomy was made on the left hemisphere over the barrel cortex (stereotaxic coordinates: 1.0–4.0 mm caudal to the bregma, and 4.0–7.0 mm lateral to the midline) and over the ventral posteromedial nucleus (VPm) of the thalamus (2.0–4.0 mm caudal, 2.5–3.5 mm lateral to the midline)[4]. The dura mater was then carefully removed. After the recording session, the animal was sacrificed with an overdose of sodium pentobarbital.

Electrophysiological recordings

Single–unit extracellular recordings were obtained by using either tungsten microelectrodes (5∼8 MΩ, FHC, Bowdoinham, ME) or quartz–insulated platinum/tungsten (90%/10%) microelectrodes (2∼6 MΩ, Thomas Recording, Germany). First, a microelectrode was advanced into VPm. After the principal whisker of the well–isolated VPm cell was identified, a micro–electrode was positioned perpendicular to the pial surface and advanced into the homologous barrel according to the barrel map, until a single unit was located that was homologous to the VPm barreloid and had a fairly restricted whisker input. For each thalamic cell, a shift in latency with adaptation greater than 20 ms resulted in exclusion of the cell from the study to ensure that the thalamic sample consisted solely of neurons from VPm, rather than POm[1]. A total of 32 thalamocortical pairs were recorded over the entire duration (> 1 hour) of the stimulus protocol (30 cortical neurons; 32 VPm neurons, two of which were recorded simultaneously with another VPm neuron).

A total of 19 simultaneously recorded pairs of VPm neurons were recorded utilizing a 20–channel microdrive system (Mini–Matrix, Thomas Recording, Germany). Three to five pulled and beveled quartz–insulated platinum/tungsten (90%/10%) microelectrodes (4–6 MΩ, 80 μm in diameter) were guided through a 5–channel linear microdrive head (Head05–lin–305–305–b, Thomas Recording, Germany) with 305 μm inter–electrode spacing, then positioned approximately 100 μm apart on the cortical surface through a custom–made glass guide tube (tip diameter: approximately 250 μm). Subsequently, these electrodes were slowly advanced into the brain independently at 1 μm resolution. All 19 pairs presented here were recorded when the two electrodes were in the same barreloid.

Data were collected using a 32–channel data–acquisition system (Plexon Inc., Austin, TX USA). Neuronal signals were amplified, band–pass filtered (500–5 kHz), and digitized at 40 kHz/channel. Recordings were analyzed using the OfflineSorter software suite (Plexon Inc., Austin, TX USA) to assign the recorded spike waveforms to single–units on the basis of standard template matching techniques and physiologically plausible refractory periods. All cortical cells were located at stereotaxic depths of 500–900 μm, presumably within cortical layer IV. Cortical cells were classified as regular spiking units (RSUs, putative excitatory neurons) or fast spiking units (FSUs, putative inhibitory interneurons) based on the width of action potential waveform. A recorded neuron was classified as an RSU when the initial trough was > 200 μs and the total duration of the waveform was > 850 μs (see Supplementary Fig. 1 online), and the spontaneous firing rate < 1 Hz[24]. Following this online classification, only RSUs were recorded in the subsequent stimulus presentation.

Whisker stimulation

Whiskers were trimmed at ∼12 mm from the face, and inserted into a 30 mm glass pipette fixed to the end of a calibrated multi–layered piezo–electric bimorph bending actuator (range of motion, 1 mm; bandwidth, 300 Hz; Polytec PI, Auburn, MA) positioned 10 mm from the vibrissa pad. Rostral-caudal pulse deflections consisted of exponential rising and falling phases (99% rise time, 5 ms; 99% fall time, 5 ms). Pulses with amplitude of 680μm (800 deg./s) were used as adapting stimuli (15 deflections at 12 Hz). The probe stimulus was presented as the 16th deflection of the 12 Hz stimulus, and thus there was an 83 ms delay between the last deflection of the adapting stimulus and the probe. Pulses with angular deflection velocities of 50, 100, 300, 600, 1200 deg./s were used as probe stimuli (s1–s5, respectively), where angular velocity was quantified as the average rate of rise to maximum amplitude. Note that the pulses had a fixed duration (10 ms), and thus the peak amplitude co–varied with the velocity[23]. Isolated deflections (Probe stimuli) were presented in the presence (Adapted) or absence (Non–adapted) of the adapting stimulus, forming stimulus blocks that were presented in an interleaved fashion. The interval between stimulus blocks was 5 seconds for probe stimuli preceded by adapting stimuli (i.e. 15 adapting deflections plus one probe deflection), and 1.5 seconds for probe stimuli. Stimulus blocks with different angular velocities of the probe stimulus were randomized. Each stimulus block was presented 100–120 times.

Response analysis

Mean spike count and variance were calculated from the trial-to-trial spike count in the 30 ms post–stimulus window following each deflection. As further confirmation of recording sites, response latencies for cortical and thalamic units were quantified in both the Non–adapted and Adapted states: Cortical (Non–adapted: 7.6+/−0.23 ms, Adapted: 13.3+/−0.91 ms), VPm (Non–adapted: 4.8+/−0.15 ms, Adapted: 10.9+/−0.88 ms, mean +/− SEM), consistent with cortical layer 4 RSUs and VPm neurons, respectively. Mean population spike count was defined as the mean spike count times the number of assumed neurons with identical statistics. Adaptation ratio was calculated by dividing the average spike count elicited by the last three pulses by the average spike count elicited by the first three pulses. The spike count distributions were fit to Gamma distributions (see Supplementary Note 2 online).

Ideal Observer – Detection

We first quantified the effects of adaptation on our ability to detect the presence of vibrissa deflection in the presence of noise. The noise distribution was evaluated by measuring the spontaneous spike count within a random 30 ms window within a 1 second period following the probe stimulus for the Adapted state, and within a 1 second period preceding the probe stimulus for the Non–adapted state. We utilized the parameterized distributions of the spike count for stimulus evoked activity and for non–stimulus evoked spontaneous activity (see Supplementary Fig. 3a online), and applied classical signal detection theory[21, 22]. The receiver operating characteristic (ROC) curve expresses the probability of a false alarm (incorrectly attributing the activity to signal when it was actually noise) versus the probability of a hit (correctly attributing the activity to signal when it was actually signal). To summarize the performance, the area under the ROC curve (AUROC) was calculated for both Non–adapted and Adapted states.

Ideal Observer – Discrimination

The ideal observer was used to discriminate between 5 different possible stimuli (s1, s2, … s5) based on the observed activity. The spike count distribution associated with each stimulus intensity was parameterized with a Gamma distribution, with the performance of the observer determined by the amount of overlap between the different distributions. We consider the ideal observer as a Bayesian decoder utilizing maximum likelihood (ML) estimation to assign an observed response to a particular stimulus intensity. The likelihood function for a particular stimulus s_i is denoted $p(r|s_i)$, where r is the observed spike count. Therefore, $p(s_i|r) = p(r|s_i)*p(s_i)/p(r)$. Note that for the case in which the stimuli are presented with equal probability, the ideal observer assigns the observation to the distribution for which the likelihood function is maximal. The performance matrix is a 5×5 matrix in which the (i,j) element is the probability of assigning the observed response to stimulus s_j when the real stimulus is s_i. The overall performance of the decoder is the sum of all diagonal elements of the performance matrix.

After we parameterized the Gamma distributions of neural activity, the theoretical performance of the ideal observer using the Bayesian decoding strategy was determined. The probability that the Bayesian decoder chooses s_i when the stimulus presented was actually s_j is the area of the region of $p(r|s_j)$ in which the $p(r|s_i)$ is maximal (Supplementary Fig. 4 online). Percent change in discrimination performance was calculated as the change in performance from the Non–adapted to Adapted states, divided by the performance in the Adapted state.

Simulation

A leaky integrate–and–fire model was used in all simulations. The model neuron had a resting potential of $V_{rest} = -70$ mV and membrane time constant of 5 ms. When the membrane potential reached −55 mV, the model neuron fired an action potential and was reset to −65 mV. Upon arrival of a presynaptic spike, an EPSC (0.4 nA, exponentially decaying with a time constant of 0.25 ms) was injected into the model neuron, whose membrane had a conductance of 2.86 nS (350 MΩ). White synaptic noise (maximum amplitude: 0.04 nA) was added to adjust the variance in trial–to–trial spike count while

maintaining the same mean spike count, tuned to match our experimental observations. The integration window of the model neuron was normally distributed across trials, with a mean +/− standard deviation of 12+/−2 ms in the Non–adapted state, and 22+/−2 ms in the Adapted state[20]. Thalamic spikes that arrive later than the integration window were discarded. To generate the thalamic input to the integrate–and–fire model of Fig. 6d, all thalamic spikes across all experimentally recorded neurons in response to a specific stimulus were pooled. For each simulated trial, 10 thalamic responses were randomly selected from the pool, and used as input to the model. This was repeated for 3200 trials, to generate an amount of simulated data comparable to that of the experimental data (across all cells and trials). Note that recent studies have suggested that the number of thalamic inputs to recipient cortical layer 4 neurons may be more on the order of 100[25]. Since we constructed the VPm population from randomly selected trials of the recorded VPm inputs, we are limited by the number of recorded trials. However, when the analysis was repeated for 20 and 30 trials, there was no significant change in the results, suggesting that our smaller sample captures the essential relationship. Note that all simulations were repeated with a quadratic (squaring) nonlinearity in the output of the integrate–and–fire model[55], resulting in no qualitative difference. Further, simulations were repeated while including a simple model of synaptic depression[2]. Specifically, during the adapted state, we attenuated the EPSC caused by the thalamic spike by 40%, but this resulted in qualitatively very similar results to those shown here.

Cross–correlation Analysis

A subset of thalamocortical pairs was identified as likely to be monosynaptically connected through cross–correlation analysis. Given the low spontaneous firing rates of neurons in primary somatosensory cortex, each pair was weakly driven with a 700 μm amplitude 4 Hz sinusoidal deflection of the principal whisker[24], [25]. A thalamocortical pair was identified as monosynaptically connected based on a sharp peak in the cross–correlogram at a very short (∼2 ms) latency[15], [24]. Due to the high degree of connectivity between neurons in a VPm barreloid and neurons in the corresponding layer 4 barrel[25], it is likely that more of the pairs were monosynaptically connected than those conservatively reported here. Cross–correlation analysis was also used for stimulus–evoked activity to assess the synchrony across thalamocortical pairs, and the effects of adaptation on this relationship. The cross–correlogram was constructed in the same manner as above, and the synchrony was defined as the central area under the cross–correlogram within a synchrony window as in Temereanca et al.[19]. The shuffled cross–correlogram was also generated for comparison[24] (Supplementary Fig. 10 online).

Statistical Analysis

Shapiro–Wilk normality test was used to assess the normality of data prior to performing statistical tests. If the samples were normally distributed, Student's t–test was used. Otherwise, the Mann–Whitney U test was used for unpaired samples, and the Wilcoxon signed–rank test was used for paired samples.

Supplementary Material

Refer to Web version on PubMed Central for supplementary material.

Acknowledgments

We would like to thank Jose–Manuel Alonso for comments at various points of this work, and Daniel Millard for assistance in calibration and testing of the piezo–electric stimulator. This work was supported by the National Institutes of Health (NIH R01NS48285).

References

1. Ahissar E, Sosnik R, Haidarliu S. Transformation from temporal to rate coding in a somatosensory thalamocortical pathway. Nature. 2000; 406:302–306. [PubMed: 10917531]
2. Chung S, Li X, Nelson SB. Short-Term Depression at Thalamocortical Synapses Contributes to Rapid Adaptation of Cortical Sensory Responses In Vivo. Neuron. 2002; 34:437–446. [PubMed: 11988174]
3. Higley MJ, Contreras D. Balanced Excitation and Inhibition Determine Spike Timing during Frequency Adaptation. J Neurosci. 2006; 26:448–457. [PubMed: 16407542]
4. Khatri V, Hartings JA, Simons DJ. Adaptation in Thalamic Barreloid and Cortical Barrel Neurons to Periodic Whisker Deflections Varying in Frequency and Velocity. J Neurophysiol. 2004; 92:3244–3254. [PubMed: 15306632]
5. Maravall M, Petersen RS, Fairhall AL, Arabzadeh E, Diamond ME. Shifts in Coding Properties and Maintenance of Information Transmission during Adaptation in Barrel Cortex. PLoS Biology. 2007; 5:e19. [PubMed: 17253902]
6. Fairhall AL, Lewen GD, Bialek W, de Ruyter van Steveninck RR. Efficiency and ambiguity in an adaptive neural code. Nature. 2001; 412:787–792. [PubMed: 11518957]
7. Barlow, H. Possible principles underlying the transformation of sensory messages. In: R, WA., editor. Sensory communication. MIT Press; Cambridge (Massachusetts): 1961. p. 217-234.
8. Goble AK, Hollins M. Vibrotactile adaptation enhances frequency discrimination. J Acoust Soc Am. 1994; 96:771–780. [PubMed: 7930078]
9. Goble AK, Hollins M. Vibrotactile adaptation enhances amplitude discrimination. The Journal of the Acoustical Society of America. 1993; 93:418–424. [PubMed: 8423258]
10. Tannan V, Simons S, Dennis RG, Tommerdahl M. Effects of adaptation on the capacity to differentiate simultaneously delivered dual-site vibrotactile stimuli. Brain Research. 2007; 1186:164–170. [PubMed: 18005946]
11. Tommerdahl M, et al. Human vibrotactile frequency discriminative capacity after adaptation to 25 Hz or 200 Hz stimulation. Brain Research. 2005; 1057:1–9. [PubMed: 16140284]
12. Crick F. Function of the thalamic reticular complex: the searchlight hypothesis. Proceedings of the National Academy of Sciences. 1984; 81:4586–4590.
13. Steriade M, McCormick DA, Sejnowski TJ. Thalamocortical oscillations in the sleeping and aroused brain. Science. 1993; 262:679–685. [PubMed: 8235588]
14. Lesica NA, Stanley GB. Encoding of Natural Scene Movies by Tonic and Burst Spikes in the Lateral Geniculate Nucleus. J Neurosci. 2004; 24:10731–10740. [PubMed: 15564591]
15. Swadlow HA, Gusev AG. The impact of 'bursting' thalamic impulses at a neocortical synapse. Nat Neurosci. 2001; 4:402–408. [PubMed: 11276231]
16. Usrey WM, Alonso JM, Reid RC. Synaptic Interactions between Thalamic Inputs to Simple Cells in Cat Visual Cortex. J Neurosci. 2000; 20:5461–5467. [PubMed: 10884329]
17. Roy SA, Alloway KD. Coincidence Detection or Temporal Integration? What the Neurons in Somatosensory Cortex Are Doing. J Neurosci. 2001; 21:2462–2473. [PubMed: 11264320]
18. Pinto DJ, Brumberg JC, Simons DJ. Circuit Dynamics and Coding Strategies in Rodent Somatosensory Cortex. J Neurophysiol. 2000; 83:1158–1166. [PubMed: 10712446]

19. Temereanca S, Brown EN, Simons DJ. Rapid Changes in Thalamic Firing Synchrony during Repetitive Whisker Stimulation. J Neurosci. 2008; 28:11153–11164. [PubMed: 18971458]
20. Gabernet L, Jadhav SP, Feldman DE, Carandini M, Scanziani M. Somatosensory Integration Controlled by Dynamic Thalamocortical Feed-Forward Inhibition. Neuron. 2005; 48:315–327. [PubMed: 16242411]
21. Britten KH, Shadlen MN, Newsome WT, Movshon JA. The analysis of visual motion: a comparison of neuronal and psychophysical performance. J Neurosci. 1992; 12:4745–4765. [PubMed: 1464765]
22. Stuttgen MC, Schwarz C. Psychophysical and neurometric detection performance under stimulus uncertainty. Nat Neurosci. 2008; 11:1091–1099. [PubMed: 19160508]
23. Ganmor E, Katz Y, Lampl I. Intensity-Dependent Adaptation of Cortical and Thalamic Neurons Is Controlled by Brainstem Circuits of the Sensory Pathway. Neuron. 2010; 66:273–286. [PubMed: 20435003]
24. Bruno RM, Simons DJ. Feedforward Mechanisms of Excitatory and Inhibitory Cortical Receptive Fields. J Neurosci. 2002; 22:10966–10975. [PubMed: 12486192]
25. Bruno RM, Sakmann B. Cortex Is Driven by Weak but Synchronously Active Thalamocortical Synapses. Science. 2006; 312:1622–1627. [PubMed: 16778049]
26. Wilent WB, Contreras D. Stimulus-dependent changes in spike threshold enhance feature selectivity in rat barrel cortex neurons. J Neurosci. 2005; 25:2983–2991. [PubMed: 15772358]
27. Schneidman E, Berry MJ, Segev R, Bialek W. Weak pairwise correlations imply strongly correlated network states in a neural population. Nature. 2006; 440:1007–1012. [PubMed: 16625187]
28. Wang HP, Spencer D, Fellous JM, Sejnowski TJ. Synchrony of Thalamocortical Inputs Maximizes Cortical Reliability. Science. 2010; 328:106–109. [PubMed: 20360111]
29. Heiss JE, Katz Y, Ganmor E, Lampl I. Shift in the balance between excitation and inhibition during sensory adaptation of S1 neurons. J Neurosci. 2008; 28:13320–13330. [PubMed: 19052224]
30. Boloori AR, Jenks RA, Desbordes G, Stanley GB. Encoding and Decoding Cortical Representations of Tactile Features in the Vibrissa System. J Neurosci. 2010; 30:9990–10005. [PubMed: 20668184]
31. Womelsdorf T, Fries P, Mitra PP, Desimone R. Gamma-band synchronization in visual cortex predicts speed of change detection. Nature. 2006; 439:733–736. [PubMed: 16372022]
32. Butts DA, et al. Temporal precision in the neural code and the timescales of natural vision. Nature. 2007; 449:92–95. [PubMed: 17805296]
33. Khatri V, Bruno RM, Simons DJ. Stimulus-Specific and Stimulus-Nonspecific Firing Synchrony and Its Modulation by Sensory Adaptation in the Whisker-to-Barrel Pathway. J Neurophysiol. 2009; 101:2328–2338. [PubMed: 19279146]
34. Hartings JA, Temereanca S, Simons DJ. Processing of Periodic Whisker Deflections By Neurons in the Ventroposterior Medial and Thalamic Reticular Nuclei. J Neurophysiol. 2003; 90:3087–3094. [PubMed: 14615426]
35. Romo R, Hernández A, Zainos A, Salinas E. Correlated Neuronal Discharges that Increase Coding Efficiency during Perceptual Discrimination. Neuron. 2003; 38:649–657. [PubMed: 12765615]
36. Zohary E, Shadlen MN, Newsome WT. Correlated neuronal discharge rate and its implications for psychophysical performance. Nature. 1994; 370:140–143. [PubMed: 8022482]
37. Carvell GE, Simons DJ. Biometric analyses of vibrissal tactile discrimination in the rat. J Neurosci. 1990; 10:2638–2648. [PubMed: 2388081]
38. von Heimendahl M, Itskov PM, Arabzadeh E, Diamond ME. Neuronal Activity in Rat Barrel Cortex Underlying Texture Discrimination. PLoS Biology. 2007; 5:e305. [PubMed: 18001152]
39. Ritt JT, Andermann ML, Moore CI. Embodied Information Processing: Vibrissa Mechanics and Texture Features Shape Micromotions in Actively Sensing Rats. Neuron. 2008; 57:599–613. [PubMed: 18304488]
40. Wolfe J, et al. Texture Coding in the Rat Whisker System: Slip-Stick Versus Differential Resonance. PLoS Biol. 2008; 6:e215. [PubMed: 18752354]

41. Jadhav SP, Wolfe J, Feldman DE. Sparse temporal coding of elementary tactile features during active whisker sensation. Nat Neurosci. 2009; 12:792–800. [PubMed: 19430473]
42. Arabzadeh E, Panzeri S, Diamond ME. Deciphering the spike train of a sensory neuron: counts and temporal patterns in the rat whisker pathway. J Neurosci. 2006; 26:9216–9226. [PubMed: 16957078]
43. Berg RW, Kleinfeld D. Rhythmic Whisking by Rat: Retraction as Well as Protraction of the Vibrissae Is Under Active Muscular Control. J Neurophysiol. 2003; 89:104–117. [PubMed: 12522163]
44. Mehta SB, Whitmer D, Figueroa R, Williams BA, Kleinfeld D. Active Spatial Perception in the Vibrissa Scanning Sensorimotor System. PLoS Biology. 2007; 5:e15. [PubMed: 17227143]
45. Krupa DJ, Matell MS, Brisben AJ, Oliveira LM, Nicolelis MAL. Behavioral Properties of the Trigeminal Somatosensory System in Rats Performing Whisker-Dependent Tactile Discriminations. J Neurosci. 2001; 21:5752–5763. [PubMed: 11466447]
46. Gerdjikov TV, Bergner CG, Stüttgen MC, Waiblinger C, Schwarz C. Discrimination of Vibrotactile Stimuli in the Rat Whisker System: Behavior and Neurometrics. Neuron. 2010; 65:530–540. [PubMed: 20188657]
47. Jenks RA, Vaziri A, Boloori Ar, Stanley GB. Self-motion and the shaping of sensory signals. J Neurophysiol. 2010; 103:2195–2207. [PubMed: 20164407]
48. Desbordes G, et al. Timing Precision in Population Coding of Natural Scenes in the Early Visual System. PLoS Biol. 2008; 6:e324. [PubMed: 19090624]
49. Goard M, Dan Y. Basal forebrain activation enhances cortical coding of natural scenes. Nat Neurosci. 2009; 12:1444–1449. [PubMed: 19801988]
50. Stoelzel CR, Bereshpolova Y, Swadlow HA. Stability of thalamocortical synaptic transmission across awake brain states. J Neurosci. 2009; 29:6851–6859. [PubMed: 19474312]
51. Castro-Alamancos MA. Role of Thalamocortical Sensory Suppression during Arousal: Focusing Sensory Inputs in Neocortex. J Neurosci. 2002; 22:9651–9655. [PubMed: 12427819]
52. Konig P, Engel AK, Singer W. Integrator or coincidence detector? The role of the cortical neuron revisited. Trends Neurosci. 1996; 19:130–137. [PubMed: 8658595]
53. Luna R, Hernandez A, Brody CD, Romo R. Neural codes for perceptual discrimination in primary somatosensory cortex. Nat Neurosci. 2005; 8:1210–1219. [PubMed: 16056223]
54. Khatri V, Simons DJ. Angularly Nonspecific Response Suppression in Rat Barrel Cortex. Cereb Cortex. 2007; 17:599–609. [PubMed: 16632642]
55. Gerstner, W.; Kistler, WM. Spiking Neuron Models: Single Neurons, Populations, Plasticity. Cambridge University Press; 2002.

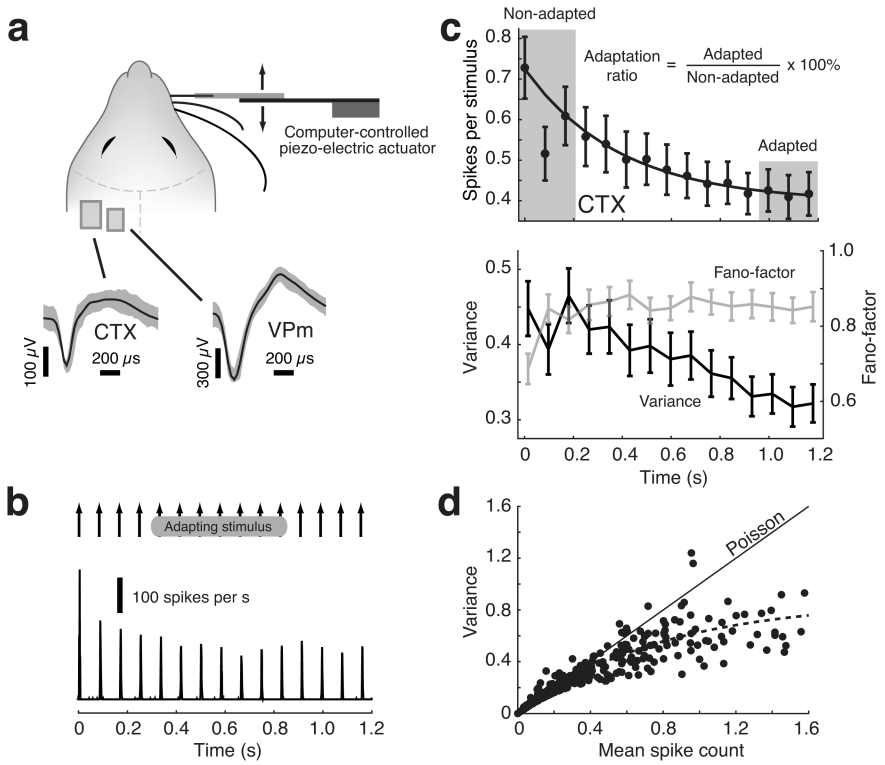

Figure 1. Statistical properties of cortical response adapt to vibrissa deflections

a. Single–unit extracellular recordings were made during movement of the identified primary vibrissa in the rostral–caudal plane using a computer–controlled piezo–electric bending actuator. Shown are example waveforms from recordings in the ventral posteromedial nucleus (VPm) thalamus (right) and cortical layer 4 (left). **b.** In response to a 12 Hz sequence of punctate vibrissa deflections (15 cycles, 800 deg./sec – see Methods), cortical neurons strongly adapt. Shown is the peri–stimulus time histogram (PSTH, 2 ms binsize) for a typical cortical regular spiking unit (RSU). **c.** Top: The mean spike count (in 30 ms bin following each deflection) across the sample (n=30 cortical RSUs). Inset shows Adaptation Ratio, defined as the ratio of the mean spike count in the Adapted to Non–adapted states (67% for the cortical RSUs). Bottom: The corresponding spike count variance (left axis) and fano–factor (variance/mean, right axis), across the cortical sample. **d.** In general, the cortical response was sub–Poisson, with trial–to–trial spike count variance significantly less than the mean for high spike counts. Note that each data point represents the response in a 30 ms window following the probe stimulus. Dashed line shows exponential fit of relationship, as compared to the Poisson case for which the variance equals the mean (solid line). Error bars are +/− 1 standard error of the mean (SEM).

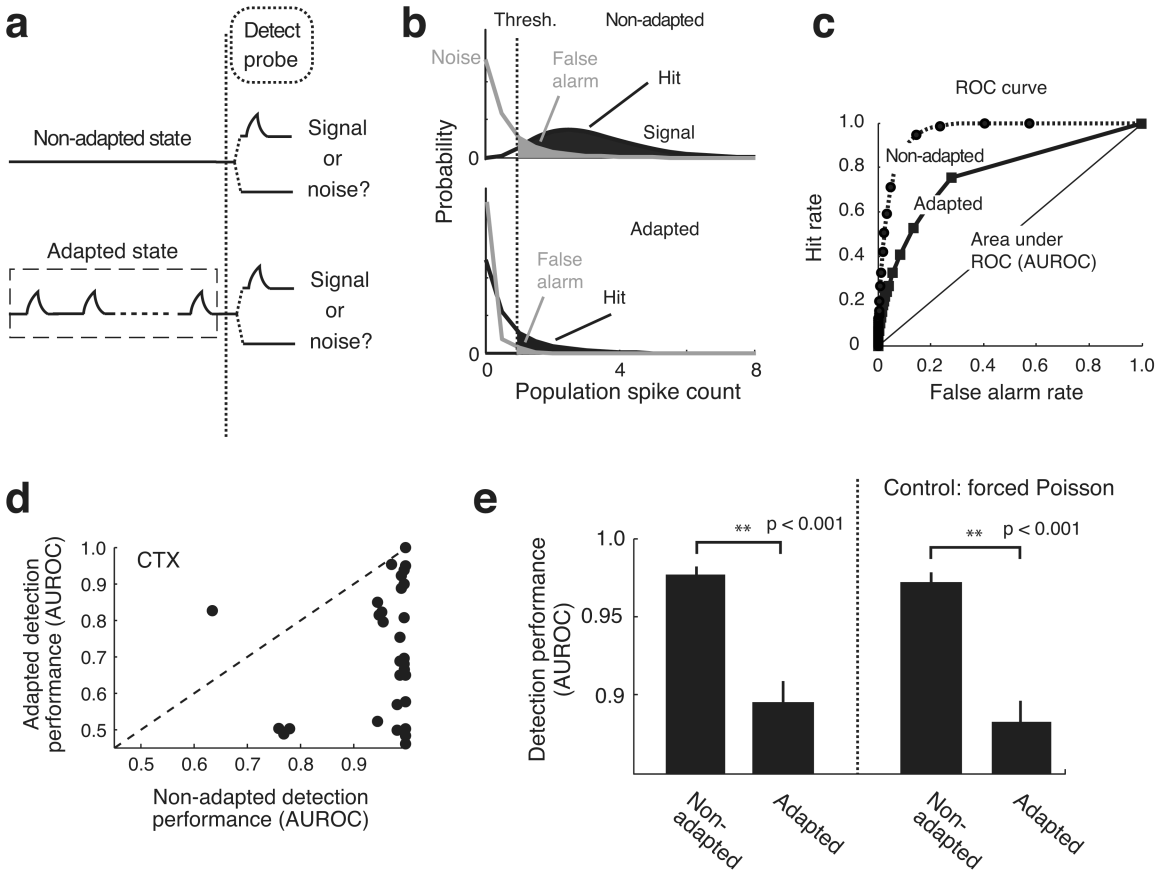

Figure 2. Adaptation degrades stimulus detection for ideal observer of cortical activity

a. Observer attributes response to "signal" or "noise", in the presence (Adapted) and absence (Non–adapted) of a preceding adapting stimulus (15 cycles of a 12 Hz sequence of a punctate deflection at 800 deg./sec). **b.** Variations in spike count from trial–to–trial establish distributions for the signal and the noise (parametric fits of raw data, Supplementary Note 2), in both the Non–adapted (top) and Adapted (bottom) states. Above a threshold, the observed spike count was attributed to signal and below to noise. The mean spontaneous firing rate decreased from 0.68±0.093 Hz in the Non–adapted state to 0.42±0.064 Hz in the Adapted state (Mean±SEM, $p<0.01$, Wilcoxon signed–rank test). **c.** The area under the receiver operating characteristic (ROC) curve was used as a metric for overall performance (AUROC), greater for the Non–adapted (dotted) case as compared to the Adapted (solid). **d.** Performance (AUROC) in the detection task in the Non–adapted versus Adapted states (n=30 cortical RSUs) for the lowest velocity used for the probe. Dashed is the unity line. **e.** Detection performance was significantly better in the Non–adapted state as compared to Adapted ($p<0.001$, Wilcoxon signed–rank test). Shown are the performance results for the entire range of probe velocities. Control is the resultant performance when the spike count variance was forced to equal that of the experimentally observed mean spike count in the Non–adapted and Adapted states (Supplementary Note 1). Error bars are +/− 1 SEM.

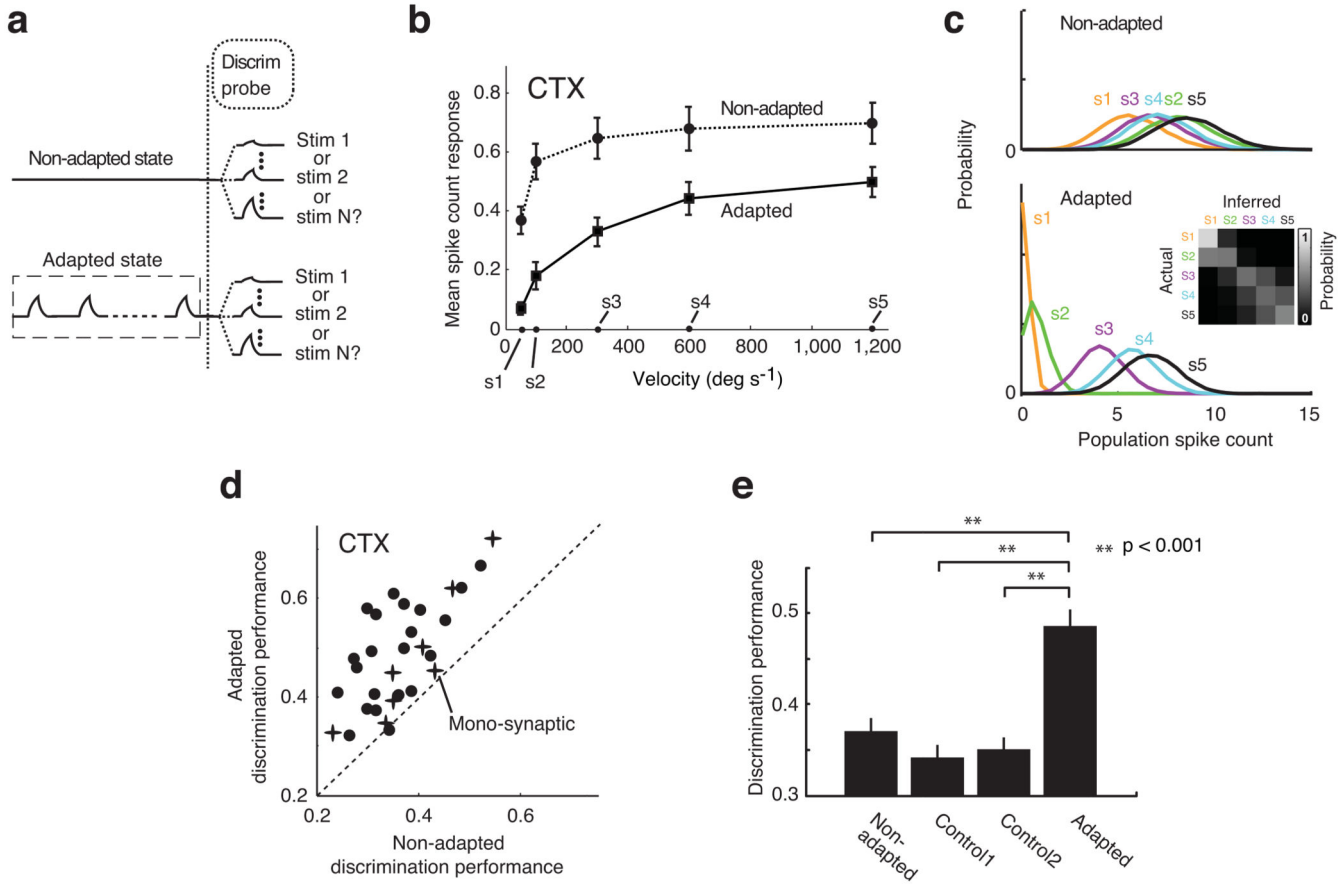

Figure 3. Adaptation enhances cortical discriminability

a. Observer attributed spike count to one of several possible stimuli, in the presence (Adapted) and absence (Non–adapted) of a preceding adapting stimulus. **b.** Mean sensitivity of the cortical response to the deflection velocity in the Non–adapted (dotted) and Adapted (solid) states (n=30 cortical RSUs). The velocities to be discriminated between (s1–s5) are noted on the horizontal axis. **c.** Population spike count distributions for a typical cortical neuron for the velocities (s1–s5) in the Non–adapted (top) and Adapted (bottom) states. Adaptation attenuated the response, but also separated the distributions. Shown in the inset is the performance matrix (see Methods). **d.** The overall discriminability performance was quantified as the fraction of correct identifications. The crosses represent cortical neurons that were identified as monosynaptic recipients of VPm inputs (Fig. 5). **e.** Discrimination performance was significantly better in the Adapted state as compared to the Non–adapted state (n=30 cortical RSUs, $p<0.001$, Wilcoxon signed–rank test). The first control (Control1) is the case where the mean spike count in response to each velocity in the Non–adapted state was attenuated by deleting 33% of the spikes to match the observed overall spike count reduction with adaptation. The second control (Control2) is the case where the mean and variance in the Non–adapted state were scaled down 33% to match the spike count reduction caused by the adaptation (Supplementary Note 1). In both control cases, there was no difference in performance from the Non–adapted state. Error bars are +/− 1 SEM.

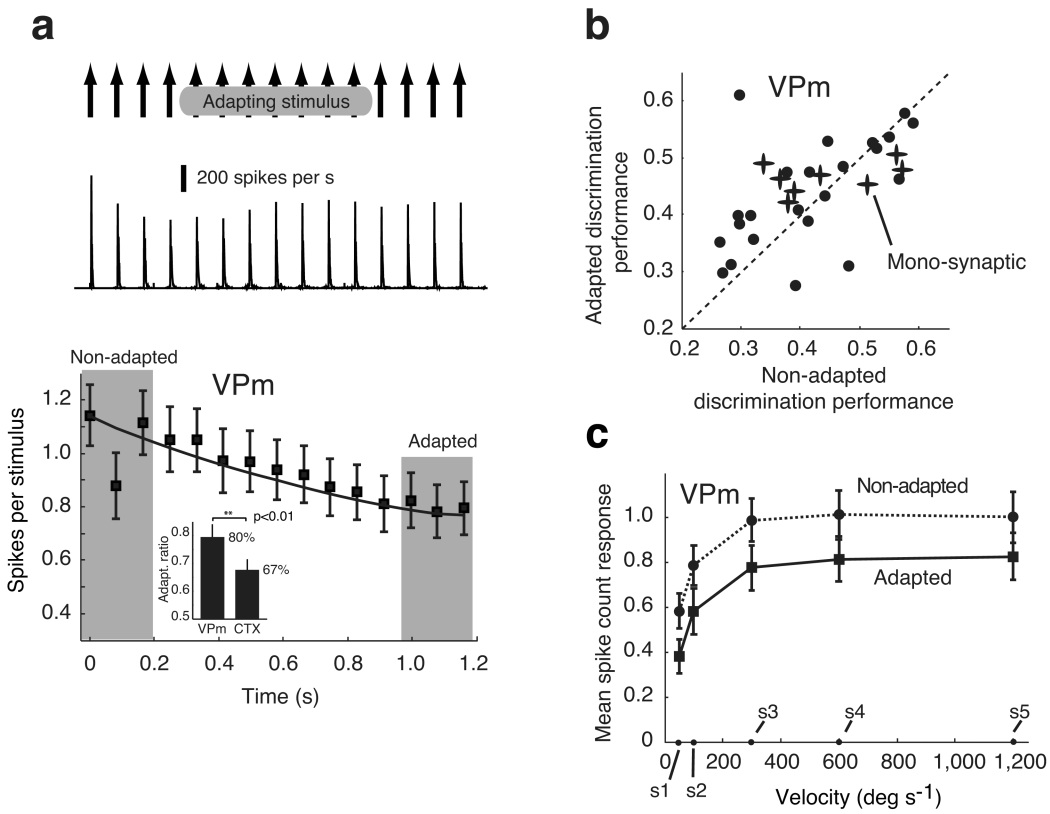

Figure 4. Cortical performance does not trivially mirror activity of thalamic projections

a. For each cortical recording, a VPm neuron in the homologous barreloid was recorded simultaneously. The VPm neurons adapted to the persistent, ongoing periodic vibrissa deflection, but exhibited less attenuation in the response (PSTH for a typical example – 1 ms bin, mean spike count across the larger sample, n=32 VPm units). The inset shows the adaptation ratio for the cortical RSUs (67%) and VPm (80%) neurons, as defined in Fig. 1. **b.** Shown is the discrimination performance in the Non–adapted versus Adapted states for the recorded VPm units (n=32). Highlighted with crosses are those that were identified as monosynaptically connected to the RSUs highlighted in Fig. 3d. Adaptation did not affect the discrimination performance for an ideal observer of VPm spike count (p=0.19, n=32, Wilcoxon signed–rank test). **c.** In contrast to cortex, the VPm curve retained its shape following adaptation, resulting in little or no change in overall sensitivity, and thus no change in performance. Error bars are +/− 1 SEM.

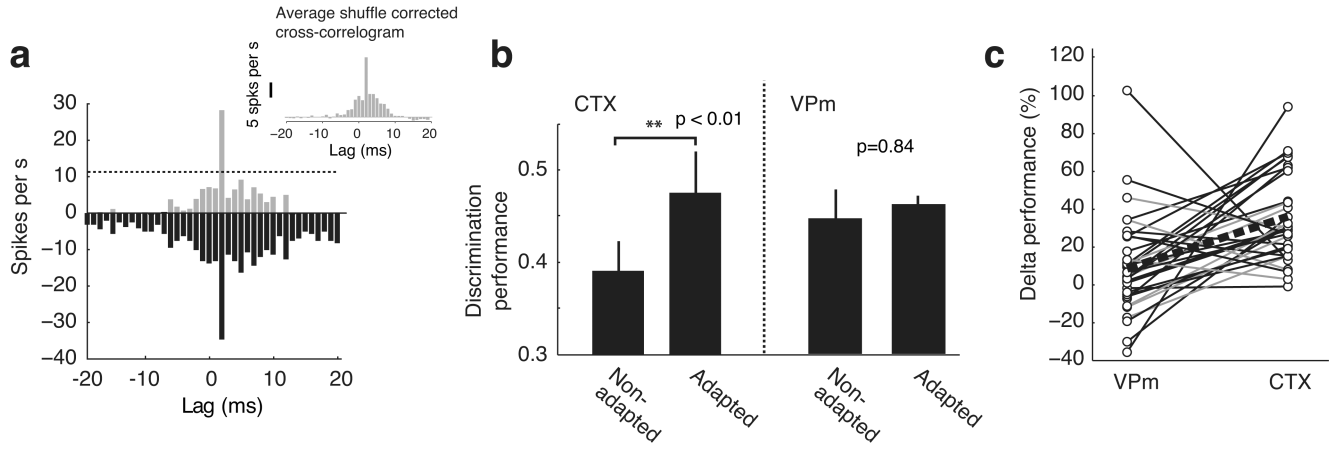

Figure 5. Detection/Discrimination performance is maintained in monosynaptically connected thalamocortical pairs

a. VPm–CTX pairs were identified as monosynaptically connected based on the presence of a statistically significant, short–latency peak in the spike train cross–correlation function for weak 4Hz sinusoidal vibrissa stimulation. Shown is an example of the raw (reflected about axis) and shuffle–corrected correlograms for a particular VPm–CTX pair, along with the corresponding >99% confidence intervals on an uncorrelated process (dotted). The inset shows the average shuffle–corrected correlogram for the 8 pairs. **b.** The results for the larger sample (Figs. 3 and 4) held for the smaller, monosynaptically connected sample. **c.** Percent change in discrimination performance from Non–adapted to Adapted states, for each VPm–CTX pair. Gray lines denote pairs identified as likely to be monosynaptically connected. Thick dashed line shows the mean performance change. Error bars are +/− 1 SEM.

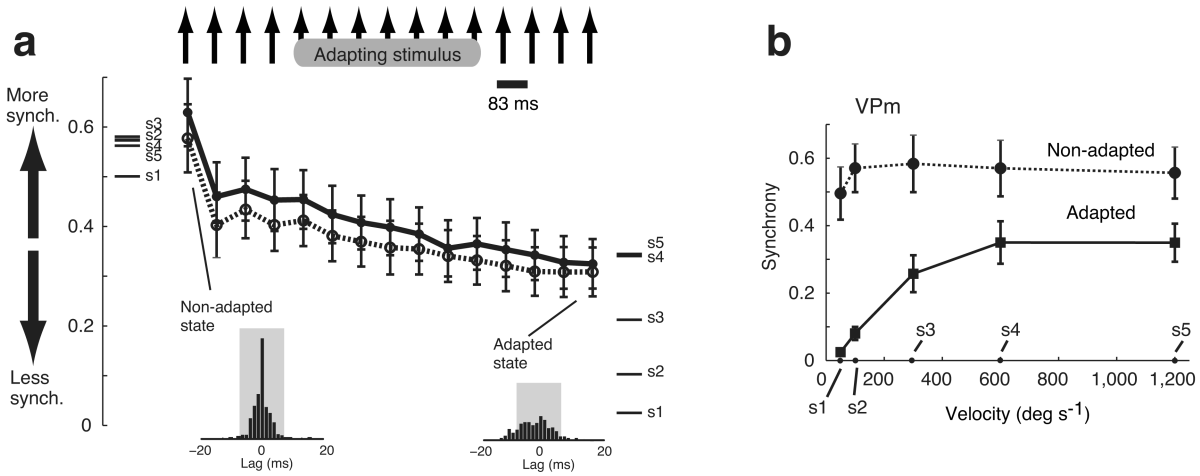

Figure 6. Thalamic population synchrony is modulated by adaptation

a. For VPm pairs recorded simultaneously, the adaptation served to reduce the timing precision across neurons, or desynchronize their firing activity (n=19 pairs). Synchrony was measured as the central area under the cross–correlogram (+/− 7.5 ms, see Supplementary Note 4 and Supplementary Fig. 10 online). Shown also are the measures of synchrony for the 5 velocities to be discriminated between, in the Non–adapted (left) and Adapted (right) states. Note that although adaptation decreased the synchrony among the VPm neurons, it facilitated an increased sensitivity of the thalamic synchrony with differences in deflection velocity. The inset shows the spike cross–correlograms in the Non–adapted and Adapted states. Note that when the trials were shuffled, the resulting synchrony in response to the velocity was unchanged (dotted line, open symbols). **b.** Synchronous firing across VPm pairs as a function of deflection velocity, in both the Non–adapted (dotted, circle) and Adapted states (solid, square).

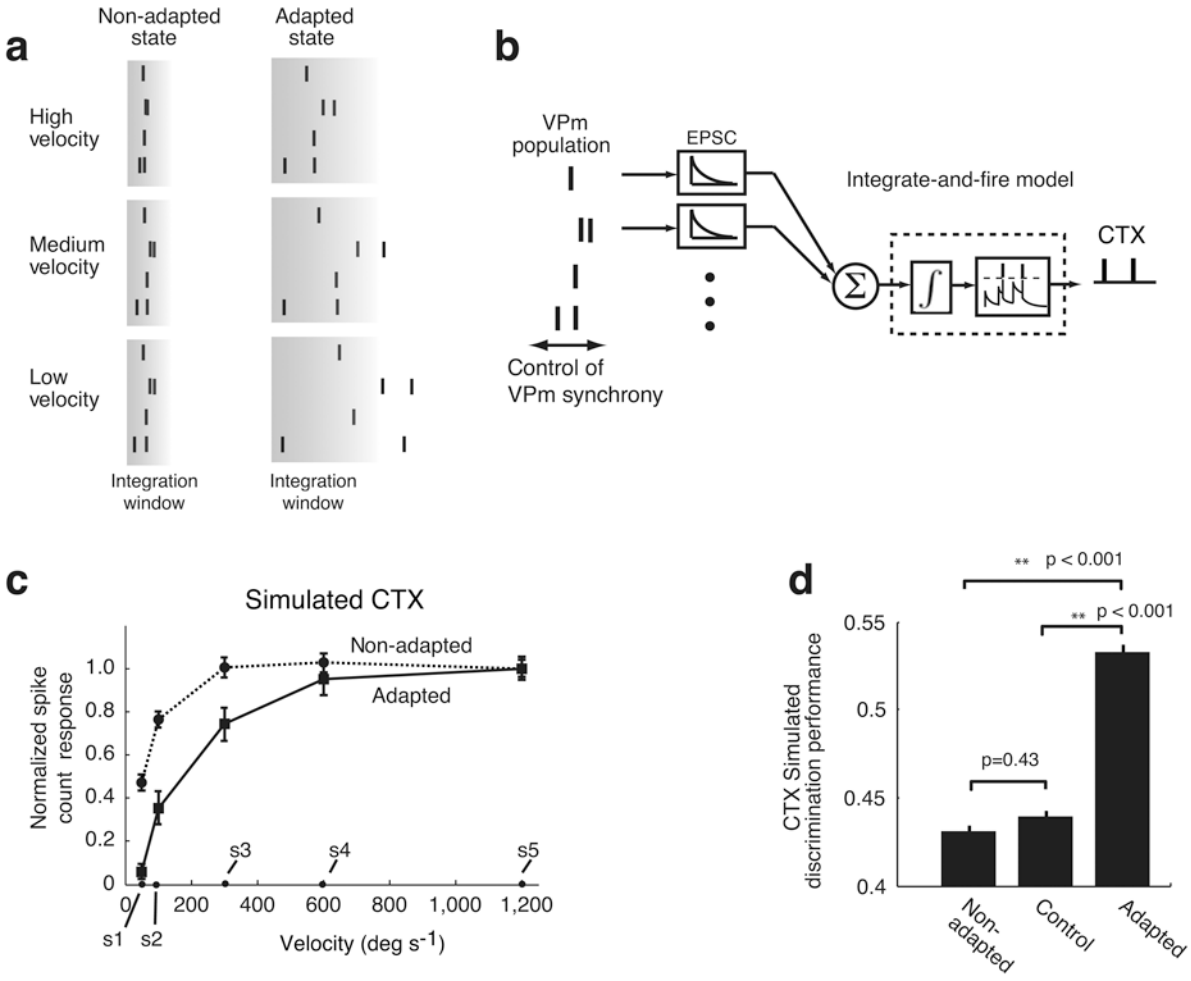

Figure 7. Thalamocortical network model predictions

a. Thalamic spiking that falls within the cortical integration window is relayed to cortex. In the Non–adapted state (left), velocity effects on synchrony of VPm activity are small, and signals are strongly relayed to cortex. In the Adapted state (right), the integration window widens, and the velocity strongly modulates the VPm synchrony. At lower velocities, VPm spiking falls outside the integration window, and fails to relay to cortex. **b.** The spiking activity from a population of VPm neurons was utilized as the input to an integrate–and–fire model of the cortical response. Firing of a VPm input generates an excitatory post–synaptic current (EPSC), the sum of which is integrated in the model to affect the cortical membrane potential. Upon crossing a threshold, the model cortical cell fires a spike, then resets. **c.** Velocity sensitivity curves for the simulated cortical response in the Non–adapted (dashed) and Adapted (solid) states, both normalized to their peak spike count. **d.** The change in thalamic synchrony with adaptation served to increase performance in discriminating between different velocities based on cortical spike count response. The control (Control) shows the case where the adaptation produced changes in the VPm spike count, as observed, but the degree of synchrony was maintained in the Non–adapted state, resulting in a loss in performance in the Adapted state. Error bars are +/− 1 SEM.